© 2024. Published by The Company of Biologists Ltd | Development (2024) 151, dev203088. doi:10.1242/dev.203088

RESEARCH ARTICLE

HUMAN DEVELOPMENT

Heterotypic interaction promotes asymmetric division of human hematopoietic progenitors

Adrian Candelas[1], Benoit Vianay[2], Matthieu Gelin[1,*], Lionel Faivre[3], Jerome Larghero[3], Laurent Blanchoin[2], Manuel Théry[1,2,‡] and Stéphane Brunet[1,‡]

ABSTRACT

Hematopoietic stem and progenitor cells (HSPCs) give rise to all cell types of the hematopoietic system through various processes, including asymmetric divisions. However, the contribution of stromal cells of the hematopoietic niches in the control of HSPC asymmetric divisions remains unknown. Using polyacrylamide microwells as minimalist niches, we show that specific heterotypic interactions with osteoblast and endothelial cells promote asymmetric divisions of human HSPCs. Upon interaction, HSPCs polarize in interphase with the centrosome, the Golgi apparatus, and lysosomes positioned close to the site of contact. Subsequently, during mitosis, HSPCs orient their spindle perpendicular to the plane of contact. This division mode gives rise to siblings with unequal amounts of lysosomes and of the differentiation marker CD34. Such asymmetric inheritance generates heterogeneity in the progeny, which is likely to contribute to the plasticity of the early steps of hematopoiesis.

KEY WORDS: Hematopoiesis, Stem cells, Niches, Microfabrication, Heterotypic interaction, Asymmetric division, Human

INTRODUCTION

Asymmetric cell division is one evolutionary conserved strategy to generate the cellular diversity adopted by stem cells. Asymmetric divisions can lead to unequal inheritance of cell fate determinants (Tajbakhsh et al., 2009) or place the two daughter cells in distinct environments providing different fate determinants (Kiger et al., 2001). In most characterized stem cells so far, asymmetry relies on the polarization of the mother cell controlled by external cues of the cell microenvironment (Daley and Yamada, 2013; Song et al., 2002; Mesa et al., 2018). These cues induce centrosome positioning in interphase, and, in turn, orientation of the mitotic spindle along the polarity axis (Venkei and Yamashita, 2018). Paradigmatic of adult stem cells, hematopoietic stem and progenitor cells (HSPCs) self-renew and differentiate into lineage-determined daughter cells, which will give rise to all cell types of the hematopoietic system (Orkin and Zon, 2008). HSPCs are retained in the bone marrow within specific niches (Schofield, 1978), where external cues modulate their homeostasis (Wilson and Trumpp, 2006; Pinho and Frenette, 2019). However, the mechanism(s) leading to asymmetric division of HSPCs has not yet been well characterized. *In vitro* HSPCs can undergo asymmetric divisions (Beckmann et al., 2007; Ting et al., 2012; Görgens et al., 2014; Florian et al., 2018; Zimdahl et al., 2014; Vannini et al., 2019; Loeffler et al., 2019). *In vitro* (Wagner et al., 2007; Nakahara et al., 2019; Xiao et al., 2009; Yu et al., 2017) or *in vivo* (Calvi et al., 2003; Lo Celso et al., 2009; Bowers et al., 2015; Christodoulou et al., 2020) investigations have shown that stromal cells, including osteoblasts and endothelial cells, can modulate HSPC proliferation and differentiation. This suggests that stromal cells may play a role in controlling asymmetric HSPC divisions (Wu et al., 2007). Nevertheless, such a role still remains hypothetical. Classical *in vitro* co-cultures are unlikely to allow the mechanisms at play to be deciphered because they inadequately recapitulate the long-term confinement encountered by HSPCs in their niches. Moreover, *in vivo* imaging of HSPC–stromal cell interactions and subsequent cell divisions has not yet been achieved. To overcome such limitations, systems of intermediate complexity have been developed (Kräter et al., 2017; Bianco et al., 2019; Braham et al., 2019; Souquet et al., 2021; Glaser et al., 2022). We have recently set up a system of microwells as minimalist niches to show that human HSPCs have the capacity to interact in interphase with specific stromal cells of the bone marrow, and polarize by reorganizing intensively their intracellular architecture (Bessy et al., 2021). Combining this system with live-cell markers, we here investigate the impact of heterotypic interactions on the mode of division of HSPCs.

RESULTS

Stromal cell interaction induces stable HSPC polarization in interphase

Non-adhesive microwells were used as culture model to overcome the limitations of classical co-culture systems for long-term imaging by preventing cells escaping from the wells (Fig. 1A,B, Fig. S1A-C, Movie 1). Microwells were coated with fibronectin, a major extracellular matrix protein in the bone marrow (Van Der Velde-Zimmermann et al., 1997; Zanetti and Krause, 2020), or seeded with either stromal cells of the hematopoietic niches (osteoblasts or endothelial cells) or skin fibroblasts as control cells (Fig. 1A).

Human cord blood CD34$^+$ cells were used to perform experiments. CD34$^+$ cells form a heterogenous population of stem and progenitor cells, but are considered as a global population representing the early steps of hematopoiesis and are referred to in the literature as HSPCs (Notta et al., 2011; Buenrostro et al., 2018).

CellTracker-labeled HSPCs were loaded at a density of one cell per well (Fig. 1A,B, Fig. S1B,C). CellTracker concentration was

[1]Human Immunology, Pathophysiology, Immunotherapy, INSERM Unit 976, Institut de Recherche St Louis, AP-HP, Hôpital Saint-Louis, Université Paris Cité, F-75010 Paris, France. [2]Cytomorpholab, University Grenoble-Alpes, CEA, CNRS, INRA, Laboratoire de Phyiologie Cellulaire & Végétale, F-38054 Grenoble, France. [3]Unité de Thérapie Cellulaire, Human Immunology, Pathophysiology, Immunotherapy, INSERM Unit 976, AP-HP, Hôpital Saint-Louis, Center of Clinical Investigations in Biotherapies of Cancer CBT501, Université Paris Cité, F-75010 Paris, France. *Present address: Cell Polarity, Migration and Cancer Unit, Institut Pasteur, Université de Paris, Equipe Labellisée Ligue 2023, F-75015 Paris, France.

‡Authors for correspondence (manuel.thery@cea.fr; stephane.brunet@inserm.fr)

A.C., 0000-0003-1922-9350; B.V., 0000-0003-1926-237X; M.G., 0000-0001-5676-4841; L.B., 0000-0001-8146-9254; M.T., 0000-0002-9968-1779; S.B., 0000-0003-1990-1477

Handling Editor: James Briscoe
Received 22 May 2024; Accepted 17 July 2024

Development (2024) 151, dev203088. doi:10.1242/dev.203088

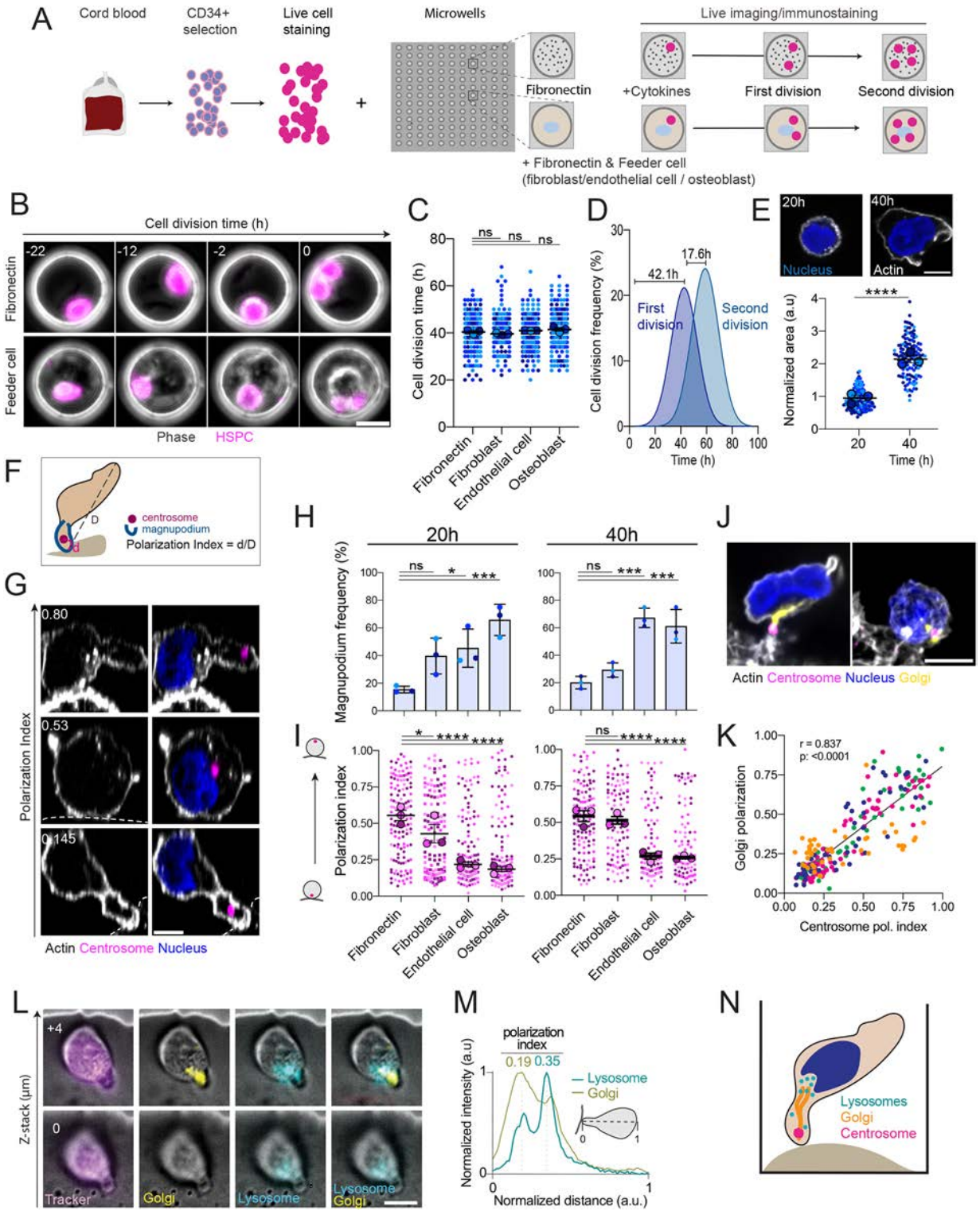

Fig. 1. See next page for legend.

optimized to preserve cell viability, cell cycle progression and proliferation (Fig. S1D,E,G). Using this system, HSPCs could be tracked over a few generations (Fig. 1B, Movie 2). Upon culture, HSPCs were observed to enlarge between 20 and 40 h, indicative of cell cycle progression (Fig. 1E). In the three culture conditions, cell division occurred at around 40 h (Fig. 1C), followed by a second division around 20 h later (Fig. 1D), indicating that the different feeder cells seeded in the microwells had no effect on HSPC cell cycle kinetics.

HSPCs cultured on fibronectin or fibroblasts had a round morphology or exhibited a dorsal uropod, at 20 h and 40 h of culture (Fig. 1F,G, Fig. S2A). In contrast, at 20 h, more than 40% of HSPCs cultured on endothelial cells or osteoblasts were elongated and anchored on the feeder cell through a magnupodium (Fonseca

Development (2024) 151, dev203088. doi:10.1242/dev.203088

Fig. 1. Bone marrow stromal cell interaction induces stable HSPC polarization during interphase. (A) Scheme of the experimental design for long-term tracking of HSPCs (co-)cultured in polyacrylamide microwells. (B) Time-lapse monitoring with transmitted light and fluorescence of live HSPCs labeled with CellTracker (magenta) in contact with fibronectin (upper row) or feeder cells (in this case osteoblasts; lower row). Time is indicated in hours relative to HSPC mitosis. Scale bar: 20 µm. (C) SuperPlot of the cell division time of HSPCs in contact with fibronectin, osteoblasts and skin fibroblasts. Each color represents a biological replicate (three biological replicates; fibronectin n_{tot}=168, fibroblasts n_{tot}=119 cells, endothelial cells n_{tot}=154, osteoblasts n_{tot}=163). For each replicate, the median value appears as a large circle of the corresponding color. Mean of the medians ±s.e.m. is shown as black bars. ns, non-significant (one-way ANOVA). (D) Gaussian fitted curves of the relative frequency for the first and second division (three biological replicates; n_{tot}=122 and n_{tot}=141 cells, respectively). The peaks of division are indicated. (E) Top: representative images of HSPCs on fibronectin at 20 h and 40 h of culture. Actin is shown in gray, nucleus in blue. Scale bar: 5 µm. Bottom: SuperPlot of the HSPC normalized area was analyzed upon culture on fibronectin at 20 h and 40 h of culture. Each color represents a biological replicate (three biological replicates; 20 h n_{cells}=141, 40 h n_{cells}=121). For each replicate, the median value appears as a large circle of the corresponding color. Mean of medians ±s.e.m. is shown as black bars. ****P≤0.0001 (Mann–Whitney U test). (F) As schematized, the HSPC polarization index was defined as the ratio between d, the distance from the site of contact to the projected centrosome point, and D, the HSPC length. (G) Representative images of HSPCs contacting either a feeder cell or fibronectin and presenting different of polarization indexes (indicated in white). Actin is shown in gray, the nucleus in blue, and the centrosome in magenta. Surfaces of contact are underlined with dashed line. Scale bar: 5 µm. (H) Percentage of HSPCs with a magnupodium at 20 h (left) and 40 h (right) of culture (three biological replicates). ns, non-significant; *P≤0.05; ***P≤0.001 (one-way ANOVA). (I) SuperPlot of HSPC polarization index at 20 h of culture (left panel; three biological replicates: fibronectin n_{tot}=142 cells, skin fibroblasts n_{tot}=125 cells, endothelial cells n_{tot}=123 cells, osteoblasts n_{tot}=142 cells) and at 40 h of culture (three biological replicates: fibronectin n_{tot}=127, skin fibroblasts n_{tot}=96 cells, endothelial cells n_{tot}=93, osteoblasts n_{tot}=91). For each replicate, the median value appears as a large circle of the corresponding color. Mean of medians±s.e.m. is shown as black bars. ns, non-significant; *P≤0.05; ****P≤0.0001 (Kruskal–Wallis ANOVA test). (J) Representative images of fixed HSPCs in contact with an osteoblast after 20 h of culture. Centrosome appears in magenta, Golgi in yellow, nucleus in blue and actin in white. Scale bar: 5 µm. (K) Correlation analysis between polarization index and Golgi polarization after 2 h (green), 4 h (magenta), 8 h (blue) and 16 h (orange) of culture on osteoblasts (one biological replicate, n_{tot}=219 cells). Spearman correlation test is indicated. (L) Representative transmitted light and fluorescence time-lapse images, at the indicated z-stack positions (white), of live HSPCs in contact with osteoblasts. HSPCs are labeled with CellTracker (magenta), Golgi tracker (yellow), and LysoBrite (cyan) for lysosome live staining. Scale bar: 5 µm. (M) Representative line-scan analysis of a polarized HPSC for lysosome and Golgi signal intensities along the cell axis (as schematized in gray). (N) Schematic representation of the architecture of a polarized HSPC interacting with a stromal cell. a.u., arbitrary units.

et al., 2010; Bessy et al., 2021). Twenty hours later, prior to cell division, 60% of them had adopted this morphology (Fig. 1F-H, Fig. S2A). At 20 and 40 h of culture, the centrosome was found within the magnupodium, located close to the site of contact with the endothelial cell or osteoblast (Fig. 1G, lower panel, Fig. S2A, Movie 3), as previously described (Bessy et al., 2021). Accordingly, the cell polarity indices, defined as the ratio between the distance from the site of contact to the centrosome and the HSPC length (Fig. 1F,G) were significantly reduced in HSPCs interacting with endothelial cells and osteoblasts, compared with HSPCs cultured on fibronectin or fibroblasts (Fig. 1I).

The effect of HSPC polarization on the spatial distribution of Golgi and lysosomes was then analyzed. The Golgi apparatus was always close to the centrosome. In the case of HSPCs with a magnupodium, it was found extending within this structure (Fig. 1J,K). Lysosomes, labeled using cell-permeable and stable fluorogenic markers, were found tightly associated with the Golgi, extending within the magnupodium (Fig. 1L,M, Fig. S2B,C, Movie 4).

Taken together, these results indicate that the interaction of HSPCs with stromal cells of the hematopoietic niches induces HSPC polarization, marked by the formation of an elongated magnupodium. Within this structure, the centrosome is located proximal to the site of interaction. The Golgi apparatus and lysosomes are confined and extend toward the cell body (Fig. 1N). Such remarkably polarized architecture is stable and maintained during cell cycle progression, until mitosis onset.

Stromal cell interaction promotes HSPC perpendicular spindle orientation at mitosis

We then investigated the impact of HSPC polarization on the subsequent mitosis. Cells were fixed at around 40 h of culture, corresponding to the peak of first mitosis (Fig. 1D). In all conditions, HSPCs were found to become rounded at mitosis onset (Fig. S3A). At prophase, in HSPCs cultured on endothelial cells or osteoblasts, centrosomes were significantly closer to the site of contact, compared with HSPCs cultured on fibroblasts or on fibronectin (Fig. S3A,B). At metaphase and anaphase, the centrosomes were located at the opposite spindle poles, thus defining the spindle axis. In HSPCs cultured on fibronectin, the spindle was oriented parallel to the bottom of the well (Fig. 2A-C, Fig. S3C,D), as previously documented (Zimdahl et al., 2014). Similarly, the spindle of HSPCs cultured on fibroblasts was oriented parallel to the surface of contact (Fig. 2A,C, Fig. S3C,D, second column). In contrast, the metaphase spindle of HSPCs interacting with endothelial cells and, more prominently, with osteoblasts was found to be oriented perpendicularly to the cell surface (Fig. 2A,C, third column, Movie 5). This perpendicularity was maintained at anaphase (Fig. S3C,D, fourth column).

These results show that the interaction of HSPCs with endothelial cells and, more drastically, with osteoblasts promotes the positioning of the spindle perpendicular to the surface of the stromal cell.

Stromal cell–HSPC interaction increases asymmetric inheritance of lysosomes

Centrosome positioning during interphase by external cues, and subsequent spindle orientation during mitosis, are hallmarks of asymmetric cell division (Venkei and Yamashita, 2018). Given that in human HSPCs asymmetric cell division has been shown to be associated with an unequal segregation of lysosomes into daughter cells (Loeffler et al., 2022), we investigated the effect of heterotypic interactions on lysosome inheritance in HSPC siblings.

The cell-permeable and stable fluorogenic marker LysoBrite™, was used to label and track HSPC lysosomes by live imaging. Upon division, CellTracker dye, used to label the whole cell, was always homogeneously segregated. In contrast, both equal and unequal LysoBrite segregations could be observed (Fig. 2D, Fig. S3E). The lysosomes were stably inherited as the LysoBrite signals were stable in time for both daughter cells (Fig. S3F). The lysosome inheritance ratio, measured as the ratio between lysosomes in the daughter cells, was significantly higher in mother HSPCs interacting with endothelial cells and osteoblasts (Fig. 2E). Setting 1.5 as a threshold value to discriminate symmetric (<1.5) versus asymmetric (≥1.5) inheritance (Loeffler et al., 2019), we determined that 60% of the HSPCs interacting with endothelial cells and osteoblasts underwent

Development (2024) 151, dev203088. doi:10.1242/dev.203088

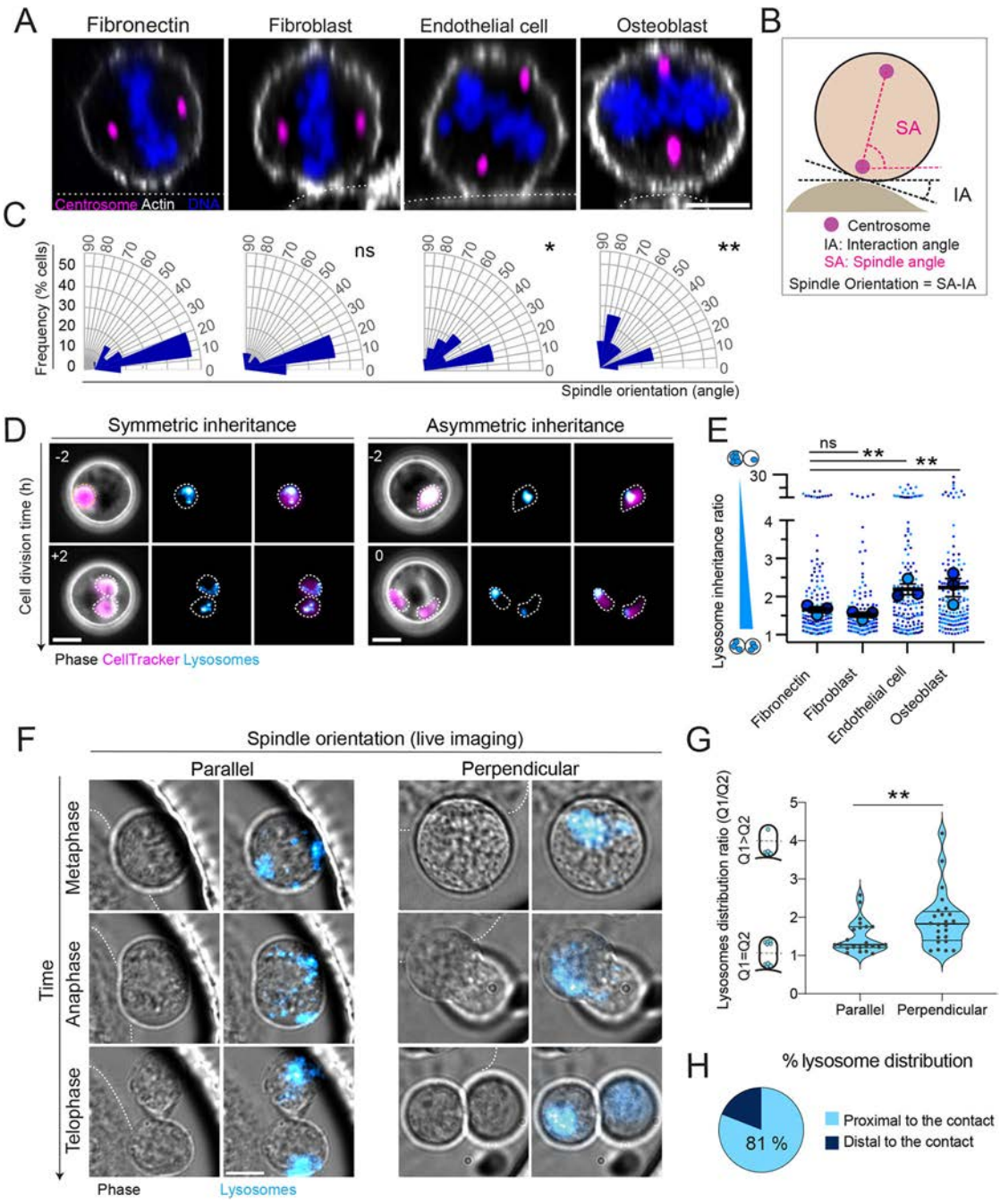

Fig. 2. Bone marrow stromal cell interaction promotes HSPC mitotic spindle orientation and asymmetric lysosome segregation. (A) Representative images of HSPCs at metaphase upon culture on fibronectin, fibroblasts, endothelial cells and osteoblasts. Actin appears in white, DNA in blue and the centrosome in magenta. Surfaces of contact are underlined with a dashed line. Scale bar: 5 µm. (B) As schematized, the spindle orientation angle was calculated as the difference between the angle defined by the spindle axis and the horizontal plane (SA), and the angle defined by the feeder cell surface (or well bottom, in the case of fibronectin) to the horizontal plane (IA). (C) Rose diagram representing the frequency of spindle orientation angles (in degrees) at metaphase (seven biological replicates; fibronectin n_{tot}=55, skin fibroblast n_{tot}=25 cells, endothelial cells n_{tot}=18 and osteoblast n_{tot}=22). ns, non-significant; *P≤0.05; **P≤0.01 (Kruskal–Wallis ANOVA test). (D) Time-lapse monitoring with transmitted light and fluorescence of live HSPCs on osteoblast, labeled with CellTracker (magenta) and LysoBrite (cyan). Representative images of LysoBrite symmetric and asymmetric inheritance are presented (left and right panels, respectively). Time is indicated in hours relative to cell division. HSPCs are outlined with white dashed lines. Scale bar: 20 µm. The corresponding extended time series can be found in Fig. S3E. (E) SuperPlot of normalized LysoBrite inheritance in the daughter cells for HSPCs in contact with fibronectin, skin fibroblasts, endothelial cells and osteoblasts. As depicted on the left, the ratio increases with the level of asymmetry. Each color represents a biological replicate (three biological replicates; fibronectin n_{tot}=151, skin fibroblasts n_{tot}=119 cells, endothelial cells n_{tot}=153 cells and osteoblasts n_{tot}=159). For each replicate, the median value appears as a large circle of the corresponding color. Mean of medians±s.e.m. shown as black bars. ns, non-significant; **P≤0.01 (Kruskal–Wallis ANOVA test). (F) Representative time frames of HSPCs on osteoblasts, taken at metaphase, anaphase and telophase (upper, middle and lower panels, respectively), with either parallel (left) or perpendicular (right) spindle orientation. LysoBrite appears in cyan. The dashed line highlights the stromal cell contact surface. Scale bar: 5 µm. (G) Violin plot representation of lysosomes ratio in HSPC halves (Q1, proximal; Q2, distal) during mitosis according to the spindle orientation (parallel n_{tot}=23, perpendicular n_{tot}=24 cells). **P≤0.01 (Mann–Whitney test). (H) Pie chart of the distribution of LysoBrite signal in cell halves, respectively proximal (light blue) and distal (dark blue) to the site of contact (n_{tot}=21 cells), of mitotic HSPCs with perpendicular spindle orientation at metaphase and anaphase.

Development (2024) 151, dev203088. doi:10.1242/dev.203088

asymmetric lysosome inheritance, compared with 40% in the case of HSPCs cultured on fibroblasts or fibronectin (Fig. S3G).

Lysosome dynamics were further assessed with cell division geometry, during the mitosis of HSPCs interacting with osteoblasts. In HSPCs dividing parallel to the osteoblast surface, lysosomes were equally distributed to the opposite cell poles. In contrast, in HSPCs dividing perpendicularly, lysosomes were found to be enriched in one of the cell poles. This enriched pole was proximal to the site of contact (Fig. 2F-H).

Taken together, these results show that HSPC interaction with stromal cells of the niches – and particularly with osteoblasts – promotes during mitosis the redistribution of lysosomes associated with spindle orientation and the asymmetric segregation of lysosomes into the daughter cells. The proximal daughter cell inherits most of the mother lysosome pool.

Stromal cell–HSPC interaction leads to HSPC asymmetric division in an SDF-1/CXCR4-dependent manner

Is there a causal link between HSPC polarization during interphase and the asymmetry of division? To address this question, HSPC polarization, cell division geometry and lysosome segregation were monitored using video microscopy in HSPCs interacting with osteoblasts, from mother cell interphase to daughter cell interphase (Fig. 3A,B). Lysosome polarization indices were measured during interphase. Based on the distribution of lysosomes in polarized HSPCs (Fig. 1M), a threshold value of 0.35 was set to discriminate polarized (<0.35) versus unpolarized (>0.35) lysosome distributions. Lysosome polarization indices were also measured during mitosis, at metaphase/anaphase (Fig. 3C), and at late telophase when daughter cells were individualized (Fig. 3D).

HSPCs that had an unpolarized lysosome distribution during interphase were mostly found to divide parallel to the osteoblast surface (Fig. 3A). During mitosis, lysosomes were redistributed within the whole rounded cell (Fig. 3A,C, blue box) and were eventually inherited symmetrically in the daughter cells (Fig. 3A,D, blue box, Movie 6). In contrast, HSPCs that had a polarized distribution of lysosomes during interphase, with lysosomes clustered in the magnupodium, mostly divided perpendicularly to the osteoblast surface (Fig. 3B). Lysosomes remained clustered close to the site of contact during mitosis (Fig. 3B,C, pink box). They were eventually asymmetrically segregated (Fig. 3B,D, pink box, Movie 7).

HSPC polarization during interphase involves the SDF-1 (CXCL12)/CXCR4 ligand/receptor couple (Bessy et al., 2021). To test whether SDF-1/CXCR4 was also involved in HSPC asymmetric division, we investigated the effect of the CXCR4 antagonist AMD3100 on HSPC division upon interaction with osteoblasts. AMD3100 was used at 50 µM, a concentration that did not impact survival, proliferation, or division kinetics (Fig. S3H-J). In these conditions, HSPC polarization was reduced during interphase (Fig. 3E). Moreover, during mitosis, the asymmetric inheritance of lysosomes was significantly decreased in AMD3100-treated cells (Fig. 3F,G). This result suggests that SDF-1/CXCR4 is involved both in HSPC polarization during interphase and in the asymmetry of HSPC division. It reinforces the causal link between HSPC polarization and further asymmetric division.

Taken together, these results show that HSPC interaction with bone marrow stromal cells is a bona fide external cue through SDF-1/CXCR4 driving asymmetric HSPC division. Interestingly, not all HSPCs respond to this cue and some undergo symmetric division. Nevertheless, once the heterotypic interaction has induced HSPC polarization with the formation of a magnupodium and the clustering of lysosomes toward the site of contact, the subsequent division is mostly marked by perpendicular spindle positioning, maintenance of the asymmetric distribution of lysosomes and final asymmetric inheritance of this organelle in the siblings.

Asymmetric division boosts HSPC sibling heterogeneity

Lysosome inheritance has been shown in human HSPCs to be predictive of cell surface marker expression in the daughter cells. In particular, CD34 expression is decreased in the daughter cell inheriting more mother cell lysosomes, whereas CD33 expression is not affected (Loeffler et al., 2022). To characterize further the daughter cells generated, we thus compared CD34 and CD33 expression in daughter cells of HSPCs cultured either on osteoblasts, which promote asymmetric divisions, or on fibronectin, as a control.

Fluorescently labeled CD34 and CD33 antibodies were added to the microwells after HSPC division (Fig. 4A) to quantify their distribution in the siblings (Fig. S4A-C). For both markers, asymmetric and symmetric distributions could be observed (Fig. 4B,C). For CD33, the ratios measured between the daughter cells (referred to as the sister ratios) were not significantly different upon culture on osteoblasts or on fibronectin (Fig. 4D). In contrast, the CD34 sister ratio was significantly higher upon culture with osteoblasts than on fibronectin (Fig. 4E). Threshold values of 1.5 and 1.25 were set to discriminate siblings with asymmetric (>1.5) and symmetric (<1.25) distributions. As far as CD33 was concerned, the two experimental conditions generated similar populations with one-third of the siblings exhibiting an asymmetric CD33 distribution (Fig. 4F). In contrast, CD34 asymmetric distributions were twice as common (41%) upon culture on osteoblasts compared with fibronectin (21%; Fig. 4G). This result indicates that heterotypic interaction with osteoblasts increases the level of CD34 asymmetric distribution in HSPC daughter cells.

Both markers were then simultaneously analyzed in the siblings (Fig. 4H). The resulting density maps in the two experimental conditions shed light on differences in sibling heterogeneity landscapes. The whole population of siblings obtained upon culture on fibronectin was found to be concentrated around low ratio values, indicative of a homogenous population. In contrast, the population resulting of HSPC culture on osteoblasts was more spread out: 75% was similar to the whole population obtained on fibronectin, whereas 25% of siblings emerged as a distinct population, with higher ratio values (Fig. 4I).

These results indicate that heterotypic interaction with osteoblasts boosts, upon mitosis, the heterogeneity of the progeny.

DISCUSSION

We here demonstrate that heterotypic interaction with bone marrow stromal cells is a genuine external cue that drives bona fide asymmetric division of human HSPCs. In the absence of polarizing external cues (i.e. cultured on fibronectin or skin fibroblasts), a fraction of HSPCs can undergo asymmetric division, indicating that HSPCs possess intrinsic properties that make them prone to asymmetry (Görgens et al., 2014; Zimdahl et al., 2014). However, heterotypic interaction with stromal cells of the vascular or endosteal niche impacts quantitatively and qualitatively the division by creating a bias toward asymmetry and by generating siblings that are more drastically divergent.

This division mode relies on a role of the centrosome, a conserved feature of asymmetric divisions in solid tissues (Venkei and Yamashita, 2018) as well as in lymphocytes (Chang et al., 2007). During interphase, the centrosome gets positioned in the vicinity of the contact site, closely associated with the Golgi apparatus and the

Development (2024) 151, dev203088. doi:10.1242/dev.203088

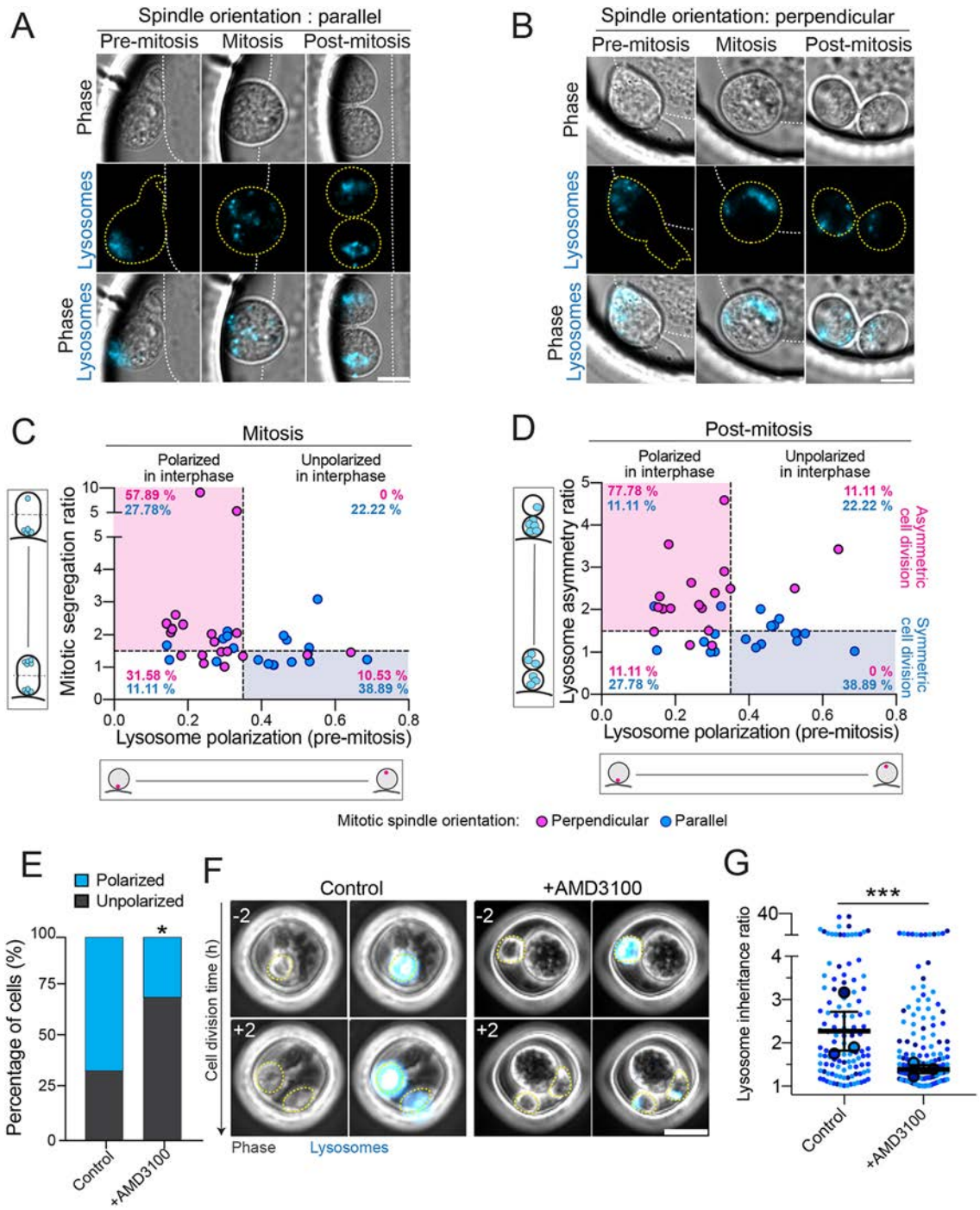

Fig. 3. HSPC polarization and perpendicular division precede asymmetric division. (A) Time-lapse monitoring with transmitted light and fluorescence (LysoBrite staining appears in cyan) of unpolarized HSPCs on osteoblasts, dividing parallel to the surface of contact. Lysosomes are symmetrically segregated. White and yellow dashed lines respectively highlight the osteoblast surface and the HSPC. Scale bar: 5 µm. (B) Time-lapse monitoring with transmitted light and fluorescence (LysoBrite staining appears in cyan) of HSPCs on osteoblasts, dividing perpendicularly to the surface of contact. Lysosomes are unequally segregated. White and yellow dashed lines respectively highlight the osteoblast surface and the HSPC. Scale bar: 5 µm. (C) Correlation plots of the lysosome segregation ratio at metaphase versus lysosome polarization at the interphase of HSPCs in contact with osteoblasts (four biological replicates; n_{tot}=38 cells). (D) Correlation plot of lysosome inheritance ratio after cell division versus lysosome polarization at the interphase preceding mitosis of HSPCs in contact with osteoblasts (four biological replicates; n_{tot}=38 cells). In C and D, HSPCs exhibiting parallel and perpendicular spindle orientation respectively appear in blue and magenta circles. Quadrant limits are presented as dashed lines to emphasize symmetric and asymmetric mitosis: 0.35 is used as a threshold value for lysosome polarization index at interphase (polarized <0.35; unpolarized >0.35) and 1.5 as a threshold value for lysosome asymmetry ratio. (E) Quantification, as percentage, of polarized (blue) versus unpolarized (gray) HSPCs, upon culture on osteoblasts, in the absence of or with 50 µM AMD3100 (three biological replicates; n_{tot}=18 cells and n_{tot}=12 cells, respectively). *P≤0.05 (binomial test, compared with control). (F) Time-lapse monitoring with transmitted light and fluorescence (LysoBrite staining appears in cyan) of HSPC division on osteoblasts with or without AMD3100 treatment. HSPCs are outlined with yellow dashed lines. Scale bar: 20 µm. (G) SuperPlot of the lysosome inheritance ratio of HSPC daughter cells in the absence or presence of AMD3100, contacting osteoblasts. Each color represents a biological replicate (three biological replicates; control n_{tot}=117 cells, AMD3100 treatment n_{tot}=128 cells). For each replicate, the median value appears as a large circle of the corresponding color. Mean of medians±s.e.m. are shown as black bars. ***P≤0.001 (Mann–Whitney U test).

Development (2024) 151, dev203088. doi:10.1242/dev.203088

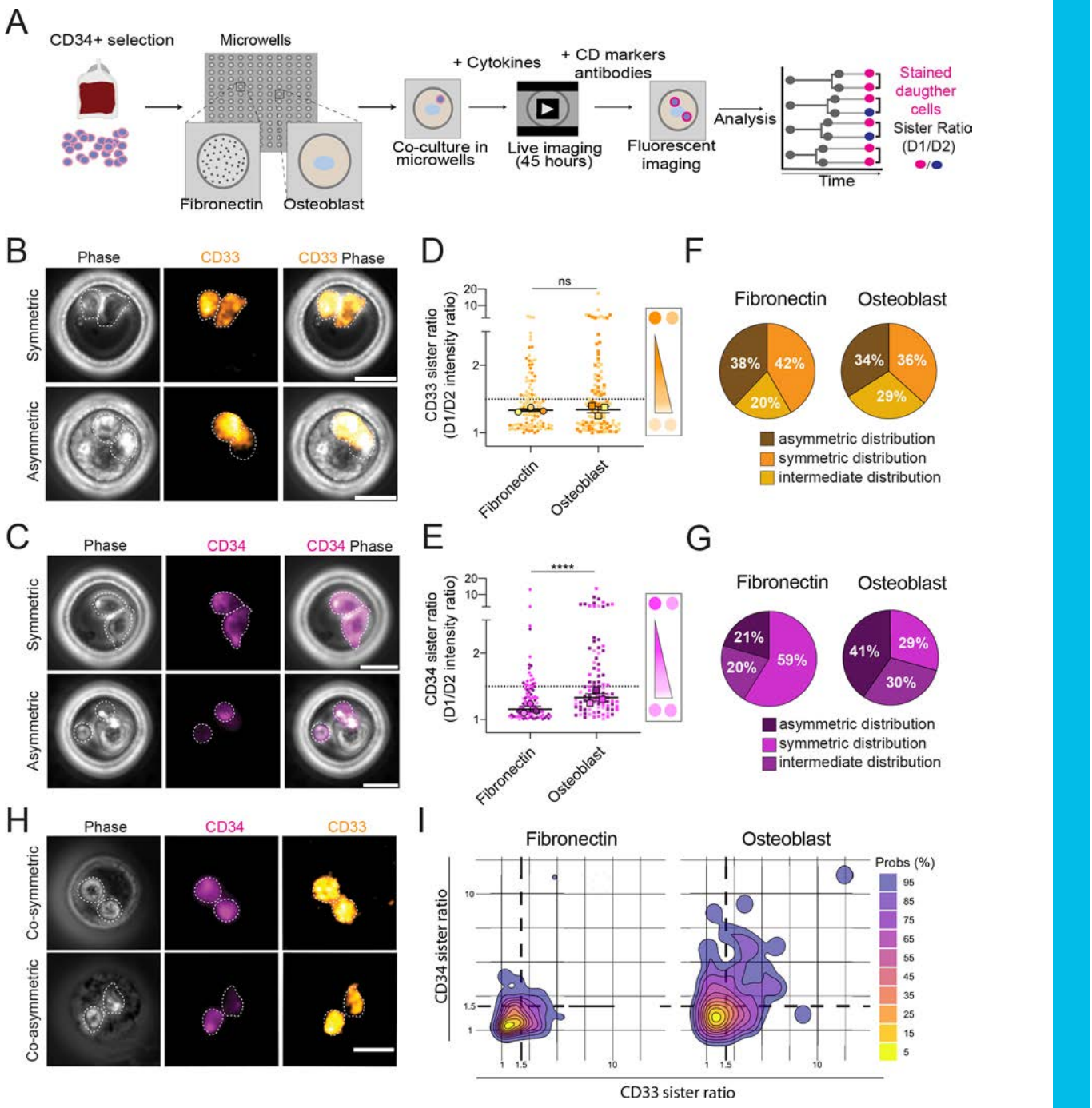

Fig. 4. Bone marrow stromal cell interaction fosters sibling heterogeneity. (A) Scheme of the experimental design for CD marker labeling of HSPC siblings and analysis. (B) Representative transmitted light and fluorescence time-lapse images of HSPCs labeled with CD33-PE, exhibiting symmetric (upper row) and asymmetric (lower row) distributions of the CD markers in the siblings. Daughter cells are outlined with white dashed lines. Scale bars: 20 µm. (C) Representative transmitted light and fluorescence time-lapse images of HSPCs labeled with CD34-APC, exhibiting symmetric (upper row) and asymmetric (lower row) distributions of the CD markers in the siblings. Daughter cells are outlined with white dashed lines. Scale bars: 20 µm. (D) SuperPlot analysis of CD33 marker signal ratios in daughter cells (sister ratio) in contact with fibronectin, and osteoblasts (three biological replicates; fibronectin n_{tot}=109, osteoblasts n_{tot}=108 cells). (E) SuperPlot analysis of CD34 marker signal ratios in daughter cells in contact with fibronectin, and osteoblasts (three biological replicates; fibronectin n_{tot}=107, osteoblasts n_{tot}=111cells). In D,E, each color represents a biological replicate. For each replicate, the median value appears as a large circle of the corresponding color. Mean of medians±s.e.m. shown as black bars. ns, non-significant; ****P≤0.0001 (Kruskal–Wallis ANOVA test). (F) Pie chart of CD33 distribution in HSPC siblings upon culture on fibronectin (left) and osteoblasts (right). (G) Pie chart representation of CD34 distribution in HSPC siblings upon culture on fibronectin (left) and osteoblasts (right). In F,G, CD marker distribution is classified into asymmetric (>1.5; dark purple for CD34 and dark brown for CD33), intermediate (≥1.25 and ≤1.5; light purple for CD34 and yellow for CD33) and symmetric (≤1.25; magenta for CD34 and orange for CD33) distributions. (H) Representative transmitted light and fluorescence time-lapse images of HSPCs co-labeled with CD34-APC (magenta) and CD33-PE (orange) exhibiting symmetric (upper row) and asymmetric (lower row) co-distributions. Daughter cells are outlined with white dashed lines. Scale bar: 20 µm. (I) Density map representation of the CD34 versus CD33 ratios in siblings produced upon HSPC division in fibronectin or osteoblast conditions (three biological replicates; fibronectin n_{tot}=100, osteoblast n_{tot}=90 cells). The color code scale used for the probability representation is depicted on the right.

Development (2024) 151, dev203088. doi:10.1242/dev.203088

lysosomes. Such organization is reminiscent of lymphocytes engaged in immune synapses (De La Roche et al., 2016). Nonetheless, whereas lymphocytes spread on their target cell, HSPCs interact with the stromal cell through an elongated and narrow magnupodium where the Golgi and lysosomes are confined (Bessy et al., 2021). Furthermore, whereas the immune synapse is maintained for minutes (Douanne and Griffiths, 2021), the magnupodium is maintained for hours. Its assembly may thus represent an efficient strategy developed by the small-sized HSPCs to sustain a robust and long-term polarization.

HSPC subsequent asymmetric division gives rise to two daughter cells positioned proximally and distally to the stromal cell. The proximal cell, positioned where the magnupodium was anchored, inherits most of the mother lysosomes. As a consequence, it has a reduced commitment to differentiation compared with the distal cell (Ito et al., 2016; Liang et al., 2020; Loeffler et al., 2022). The division thus leads to a spatial control of the position of the siblings relative to the stromal cell, which is a conserved feature of asymmetric divisions in other stem cell niches (Venkei and Yamashita, 2018). This property may account for *in vivo* observations of the organization cells into spatial clusters during blood cell differentiation (Zhang et al., 2021; Wu et al., 2024). It also may play an important role in competition mechanisms at play within the limited space of the hematopoietic niches, in physiological (Miao et al., 2022) and pathological (Colmone et al., 2008; Glait-Santar et al., 2015) contexts.

Our results indicate that the ligand/receptor pair SDF-1/CXCR4 is involved in the control of HSPC asymmetric division, similarly to what has been proposed for developing T cells (Pham et al., 2015). This original role could explain how the SDF-1/CXCR4 signaling pathway contributes to HSPC homeostasis (Kahn et al., 2004), in addition to its well-documented role in HSPC migration and retention in the niches (Lapidot et al., 2005). Similarly, SDF-1/CXCR4 dysfunction could directly affect HSPC asymmetric divisions in malignant contexts (Spoo et al., 2007; Nervi et al., 2009; Zimdahl et al., 2014).

Stem cell asymmetric division is classically considered as a binary process leading to the generation of daughter cells of distinct identities (Kuang et al., 2007; Cicalese et al., 2009). The early steps of hematopoiesis are now considered to occur as a continuum (Buenrostro et al., 2018), with the slow and progressive emergence of distinct cell populations (Tak et al., 2021). Our data support the idea that heterotypic interactions driving asymmetric divisions of stem and progenitor cells do generate siblings with different differentiation potentialities, rather than distinct identities. Such non-stereotypical asymmetric divisions are likely to participate in maintaining the plasticity of the early steps of hematopoiesis.

It is important to note that these results have been obtained on a global population of $CD34^+$ cells, which encompasses hematopoietic stem cells, multipotent progenitors and common myeloid or lymphoid progenitors. Some aspects of asymmetric division, such as niche specificities, efficiency of asymmetry, siblings' heterogeneity etc., may differ among these subpopulations. Our results pave the way to further investigations, based on the use of microfabricated niches, to decipher these differences in physiological and pathological contexts.

MATERIALS AND METHODS

Mold fabrication for microwells

The mold design and fabrication were performed as previously described (Bessy et al., 2021): microwell shape, size, and arrangement were drawn using the software CleWin and etched in the chrome layer onto a quartz photomask (Toppan Photomask). A wafer with microstructures was made on silicon. Silicon wafers were coated with a first 5-µm-thick layer of resin (SU8-3005; MicroChem; CTS), exposed to UV light at 23 mW/cm^2 (UV KUB2; Kloe) for 5 s and with a 50-µm-thick second layer (SU8-3050; MicroChem; CTS) exposed to UV light through the quartz mask at 23 mJ/cm^2 for 8 s in order to create microwells. After development (Developer SU8; MicroChem; CTS), only the exposed structures remained. The wafer was baked at 150°C for 2 h and coated with gas-phase trichloro(perfluorooctyl)silane (Sigma-Aldrich). A negative mold of the silicon wafer was created using PDMS and treated with silane in the same way as the wafer. A positive mold of PDMS was made from the first mold. This positive mold is hereafter referred to as the PDMS stamp.

Microwell fabrication

Glass coverslips were coated with a solution containing 3-(trimethoxysilyl) propylmethacrylate (Sigma-Aldrich), acetone and ethanol, in a ratio of 1:0.5:50 for 10 min. They were then baked at 120°C for 1 h. The PDMS stamp underwent plasma treatment for 30 s and was immediately apposed on the coverslip. A fresh solution of 20% 37.5/1 acrylamide/bisacrylamide (Euromedex), 1% ammonium persulfate, tetramethylethylenediamine (Sigma-Aldrich), 1% photo initiator (2-hydroxy-2-methylpropiophenone; Sigma-Aldrich) in MilliQ water was drawn by capillary action between the PDMS stamp and the glass coverslip. The sample was exposed to UV light at 23 mW/cm^2 for 5 min (Fig. S1B). After exposure, the PDMS stamp was removed in MilliQ water and washed with 70% ethanol under UV light for 1 h for sterilization. The samples were incubated in sterile PBS overnight to remove potential traces of remaining toxic compounds.

HSPC harvesting and culture

All human umbilical cord blood samples collected from normal full-term deliveries were obtained after mothers' written and informed consent, following the Helsinki's Declaration and Health Authorities. Human umbilical cord blood samples were obtained from the Cord Blood Bank of the Saint-Louis Hospital by French national law (Bioethics Law 2011-814) and under declaration to the French Ministry of Research and Higher Studies.

Mononuclear cells were collected using Ficoll separation medium (Eurobio). $CD34^+$ cells were further selected using Miltenyi magnetically activated cell sorting (MACS) columns (Miltenyi Biotech) according to the manufacturer's instructions. $CD34^+$ cells were then either put in culture or frozen at −80°C in IMDM medium (Gibco) supplemented with 10% fetal bovine serum (FBS) and 10% DMSO (WAK Chemie Medical GmbH).

Cell culture and drug treatment in microwells

The cell lines used were hFOB (osteoblasts; CRL-11372, ATCC), HUVEC-XL (endothelial cells; 191027, Lonza) and BJ (skin fibroblasts; CRL-2522, ATCC), all cultured in DMEM-F12 medium (Gibco) supplemented with 10% FBS and 1% antibiotics (AA; Gibco, 15240062). Cells were tested monthly for *Mycoplasma* contamination using MycoStripTM 50 (InvivoGen, rep-mysnc-50). Experiments were only performed with *Mycoplasma*-negative cells.

The glass bottom of the microwells was coated with 10 µg/ml of fibronectin diluted in PBS for 5 min at 37°C. Microwells were gently rinsed twice in PBS, and a droplet of 40 µl of supplemented DMEM F-12 was placed on top of the microwells, then 5000 osteoblasts, endothelial cells, or skin fibroblasts in 5 µl volume (1000 cells/µl) were directly added to the DMEM-F12 droplet in a zigzag manner. After a 30-min incubation period to allow the seeding of osteoblasts and skin fibroblasts by gravity, the dishes were filled with DMEM-F12. Following a 2-hour interval to facilitate cell spreading, 5000 HSPCs were directly seeded onto the microwells using the same method to obtain around one HSPC per well. After a 30-min incubation period to enable HSPC seeding, IMDM supplemented with 10% FBS, 1% AA, 100 ng/ml human SCF (Peprotech, 300-07), 20 ng/ml human IL-3 (Peprotech, 300-23) and 10 ng/ml human G-CSF (Peprotech, 200-02) was added to mark the starting point (t0) of the experiment (Fig. 1A, Fig. S1C).

In specific experiments, in addition to control non-treated cells, cells were treated with the CXCR4 antagonist AMD3100 (Sigma-Aldrich). HSPCs were seeded and incubated with 50 µM of AMD3100.

Development (2024) 151, dev203088. doi:10.1242/dev.203088

Cell labeling for live imaging

Coverslips with the microwells were pasted to the bottom-left 35 mm plastic dish, before the sterilization step. The medium was constantly changed every 24 h.

For live imaging labeling, HSPCs were incubated with 20 µM 6-{[N-(7-nitrobenz-2-oxa-1,3-diazol-4-yl)amino]hexanoyl}sphingosine (NBD C6-Ceramide; Invitrogen) for 30 min at 4°C for Golgi staining or with Cytopainter (Abcam) for Golgi and nucleus staining. HSPCs were incubated with 2 µM Orange CellTracker (Thermo Fisher Scientific, C34551) for 30 min or/and 1:250 LysoBrite Deep Red (Interchim, 22646) or LysoBrite NIR (Interchim, 22641) for 50 min, both at 37°C. HSPCs were rinsed and pelleted twice with HBSS (Gibco) with 10 mM HEPES (Thermo Fisher Scientific). Labeled HSPCs were finally washed in supplemented IMDM with 10 mM HEPES and, after centrifugation (90 ***g*** for 3 min), seeded in the microwells and cultured in Phenol Red-free IMDM (Thermo Fisher Scientific) with 10 mM HEPES with cytokines, FBS and AA. Images were taken every 30 min for transillumination and every 2 h for laser illumination.

CD staining of daughter cells

HSPCs were imaged using transillumination for 46 h. After 46 h and following the peak of cell divisions, anti-CD33-PE (555450, BD Biosciences) and anti-CD34-APC (55824, BD Biosciences) antibodies were added in a 1:60 ratio in 0.05% fetal human serum and PBS with 2 mM EDTA for 20 min in the microwells.

Immunofluorescence

Cells were fixed in PBS with 4% methanol-free paraformaldehyde (Electron Microscopy Sciences) for 15 min at 37°C after 20 h or 40 h of culture. Cells were permeabilized in 0.1% Triton X-100 (Sigma-Aldrich) in PBS for 20 min. Coverslips were neutralized with a solution of NH_4Cl (Sigma-Aldrich) for 10 min. The following primary antibodies and dilutions were used: rabbit anti-pericentrin (ab4448, Abcam; 1/500); human anti-giantin (A-R- H#03 TA10 hFc, Institut Curie; 1/200). Primary antibodies were incubated for 1 h. The following secondary antibodies and dilutions were used: Alexa Fluor 568-conjugated goat anti-human and 647-conjugated goat anti-rabbit (A-11011 and A-21244, respectively, Life Technologies; 1:1000). Alexa Fluor 488-conjugated phalloidin (A12379, Molecular Probes) was used to label F-actin. Finally, cells were incubated with DAPI (Sigma-Aldrich) for 10 min to stain the nucleus. The coverslips were mounted with Mowiol (Sigma-Aldrich).

Microscopy

For the measurement of polarization index and mitotic spindle orientation, images were taken using a Nikon Ti-eclipse microscope equipped with a spinning disk (Yokogawa-CSU-X1) with a 60×, 1.5 lens amplification, 1.4-NA oil objective on an electron-multiplying charge-coupled device camera (Retiga R3). MethaMorph was used as acquisition software. *z*-stacks of 0.5 µm were taken and a camera binning of 2×2 was used.

For live-cell imaging with trans and laser illumination light, an Olympus IX83 microscope equipped with a PECON CellVivo incubation system controlling temperature (37°C) and CO_2 concentration (5%) was used. Images were acquired with a 20×0.30-NA air objective on an ORCA-Flash4.0 Lite (Hamamatsu) camera and using MicroManager 1.4.21 software. A camera binning of 2×2 was used during the acquisition.

For detailed live-cell imaging of lysosome polarization and asymmetric inheritance with trans and laser illumination lights (Figs 3F, 4, Fig. S2B,C), a Nikon Ti2 Eclipse equipped with a Prime BSI Express CMOS camera (Photometrics) was used with a Nikon CFI Plan Fluor 60×/0.75 NA oil objective with 1.5 lens amplification. Okolab incubation system was used to control temperature (37°C) and CO_2 concentration (5%). Images were acquired using MicroManager 1.4.21 software. To improve the signal/noise ratio of LysoBrite and reduce laser intensity and exposition time, HSPCs were pre-stimulated for 20 h with the cytokine cocktail, then labeled with LysoBrite, and added to the microwells with osteoblasts, as previously described. After 15 h (35 h after the cytokine stimulation), microwells were positioned at the microscope and imaged (10 *z*-stacks with 4 µm step) every 15 min with a 2×2 camera binning.

Immunofluorescence quantification and analysis

Polarization index, Golgi polarization, prophase centrosome positioning, and magnupodium analysis

In the 3D images of the HSPCs, the positions of the centrosome A (Xa, Ya, Za), the point of contact B (Xb, Yb, Zb), and the most distal point on the HSPC membrane from the point of contact C (Xc, Yc, Zc), excluding thin membrane protrusions, were determined. The polarization index was calculated as d/D using ImageJ software. Distance D was defined as the length between points B and C, and distance d as the length between B and the projection of A in the D vector, using the following equation:

$$\begin{aligned} Numerator =& |(Xa - Xb) \times (Xc - Xb)| + |(Ya - Yb) \times (Yc - Yb)| \\ &+ |(Za - Zb) \times (Zc - Zb)| \end{aligned}$$

$$\begin{aligned} Denominator =& \sqrt{(Xa - Xb)^2 + (Ya - Yb)^2 + (Za - Zb)^2} \\ &\times \sqrt{(Zc - Zb)^2 + (Yc - Yb)^2 + (Zc - Zb)^2} \end{aligned}$$

$$\begin{aligned} d =& (Numerator \div Denominator) \\ &\times \sqrt{(Xa - Xb)^2 + (Ya - Yb)^2 + (Za - Zb)^2}. \end{aligned}$$

The same method was used for the analysis of Golgi polarization (taking the closest point of the Golgi to the cell membrane as 'B') and prophase centrosome polarization (polarization index ≤0.3 was taken as a proximal centrosome and >0.3 as a distal centrosome). To be considered as a bona fide magnupodium, the structure was required to be an elongated protrusion (longer than 2 µm) with a centrosome located at its tip.

For SuperPlot representation (Lord et al., 2020), each color represents a biological replicate. The median of each replicate, the mean of the medians, and the s.e.m. are presented. SuperPlots were only generated in the case of biological replicates of more than 20 cells. The normality of data distribution was tested by the Shapiro–Wilk test for further statistical test selection. The significance of the difference between populations was tested using nonparametric (Kruskal–Wallis) ANOVA and Mann–Whitney *U* test for samples that were not normally distributed, or parametric unpaired *t*-test and one-way ANOVA for normally distribution samples. All statistical analyses were performed with Prism software (GraphPad).

Mitotic spindle orientation

Mitotic cell images were resliced to visualize the centrosomes and the point of interaction with the bottom of the microwell or the osteoblast/fibroblast. For the mitotic spindle angle, the angle generated between both centrosomes with respect to the image *x*-axis was subtracted from the angle generated for the point of interaction with respect to the image *x*-axis. Graphs were generated with R (https://www.r-project.org).

Live imaging quantification and analysis

Live Golgi and lysosome polarization

A line-scan from the contact site to a more distal point was used to assess the lysosome localization with respect to the Golgi in maximum projected images. Graphs were generated with Prism software (GraphPad).

Lysosome inheritance ratio

Cells were tracked manually until division. To automate the daughter cell area selection, CellTracker images were processed with Gaussian Blur (sigma=2), Subtract Background (rolling=50), and then thresholding (Otsu dark) to create a mask for the daughter cell area. Background signal was selected manually inside the microwell for each image. Lysosome inheritance ratios were calculated in untreated images using the first time point following cell division, by dividing the brightest daughter cell by its sister, using the sum of LysoBrite pixel fluorescence values (CTCF). Ratios were therefore ≥1. Ratios <1.5 and ≥1.5 were respectively selected as indicative of symmetric and asymmetric lysosome inheritance. When both daughter cells were very close in the first time point after division, the following time point was analyzed. Manual selection of the daughter area was carried out when the automatized selection failed. Data were analyzed

with Fiji and presented as SuperPlots. Statistical analyses were performed with Prism software (GraphPad).

Lysosome polarization, mitotic spindle orientation, and inheritance ratio

Lysosome polarization in the mother cell was analyzed as described above for the time-lapse imaging before chromosome condensation, visualized by phase images. Metaphase/anaphase was analyzed in the time-lapse images, which allows the visualization of the chromosome orientation to determine mitotic spindle orientation with respect to the interaction point. In cases in which the chromosome orientation was not clear, the visualization of a cell-side attachment from metaphase to telophase was taken as a perpendicular division. Lysosome inheritance was measured after the division in the first time frame, which allows the visualization of the whole two daughter cell volumes.

CD marker ratios

Gaussian fit curves were created based on the CTCF values of HSPCs that were stained or not stained for the two CD marker signals; 95% confidence intervals of non-stained intestines were selected to determine the thresholds for positive CD34 and CD33 signals. Single mother cells were tracked manually until their division by transillumination to annotate the division time. To automate the daughter cell area selection, CD34 fluorescence images were processed with Gaussian Blur (sigma=2), Subtract Background (rolling=50) and then thresholding (Otsu dark) to create a mask for the daughter cell area. The background region was selected manually inside the microwell for each microwell. When the CD marker CTCF of both daughter cells was below the threshold, the cells were discarded. When one daughter cell was below the threshold, its CTCF was automatically converted to the value threshold and both sister cells were compared. CD marker production ratios were calculated after antibody incubation, by dividing the brightest daughter cell by its sister. Ratios were therefore always ≥ 1. Ratios ≤ 1.2 and ≥ 1.5 were respectively selected as indicative of symmetric and asymmetric distributions. Ratios between 1.2 and 1.5 were indicative of intermediate distribution. In cases in which both daughter cells were overlapping, the next time point was analyzed. Manual selection of the daughter area was carried out when the automatized selection failed. Data were analyzed with Fiji and presented as SuperPlots, or with R (https://www.r-project.org). In Fig. 4I, the corresponding density map was generated using the 'ggdensity' package (https://jamesotto852.github.io/ggdensity/, https://github.com/jamesotto852/ggdensity/). Statistical analyses were performed with Prism software (GraphPad).

Acknowledgements

We thank Sandrine Moutel and the platform TabIP of the Curie Institute (Paris) for sharing the human anti-Giantin antibody.

Competing interests

The authors declare no competing or financial interests.

Author contributions

Conceptualization: M.T., S.B.; Methodology: A.C., B.V., L.F., M.T., S.B.; Validation: L.B., M.T., S.B.; Formal analysis: A.C., B.V., M.G., M.T., S.B.; Investigation: A.C., B.V., S.B.; Resources: L.F., J.L.; Data curation: A.C.; Writing - original draft: A.C., M.T., S.B.; Writing - review & editing: A.C., M.T., S.B.; Visualization: M.T., S.B.; Supervision: L.B., M.T., S.B.; Project administration: M.T., S.B.; Funding acquisition: J.L., L.B., M.T.

Diversity and inclusion

We support inclusive, diverse and equitable conduct of research.

Funding

This work was supported by the European Research Council [Consolidator Grant 771599 (ICEBERG) to M.T. and Advanced Grant 741773 (AAA) to L.B.], the Fondation Bettencourt Schueller, the Emergence program of the Ville de Paris and the Fondation Schlumberger pour l'Education et la Recherche. A.C. received a PhD fellowship from the Fondation pour la Recherche Médicale (FDT20170437071).

Data availability

All relevant data can be found within the article and its supplementary information.

Peer review history

The peer review history is available online at https://journals.biologists.com/dev/lookup/doi/10.1242/dev.203088.reviewer-comments.pdf

References

Beckmann, J., Scheitza, S., Wernet, P., Fischer, J. C. and Giebel, B. (2007). Asymmetric cell division within the human hematopoietic stem and progenitor cell compartment: identification of asymmetrically segregating proteins. *Blood* **109**, 5494-5501. doi:10.1182/blood-2006-11-055921

Bessy, T., Candelas, A., Souquet, B., Saadallah, K., Schaeffer, A., Vianay, B., Cuvelier, D., Gobaa, S., Nakid-Cordero, C., Lion, J. et al. (2021). Hematopoietic progenitors polarize in contact with bone marrow stromal cells in response to sdf1. *J. Cell Biol.* **220**, e202005085. doi:10.1083/jcb.202005085

Bianco, J. E. R., Rosa, R. G., Congrains-Castillo, A., Joazeiro, P. P., Waldman, S. D., Weber, J. F. and Saad, S. T. O. (2019). Characterization of a novel decellularized bone marrow scaffold as an inductive environment for hematopoietic stem cells. *Biomater. Sci.* **7**, 1516-1528. doi:10.1039/c8bm01503a

Bowers, M., Zhang, B., Ho, Y., Agarwal, P., Chen, C.-C. and Bhatia, R. (2015). Osteoblast ablation reduces normal long-term hematopoietic stem cell self-renewal but accelerates leukemia development. *Blood* **125**, 2678-2688. doi:10.1182/blood-2014-06-582924

Braham, M. V. J., Li Yim, A. S. P., Garcia Mateos, J., Minnema, M. C., Dhert, W. J. A., Öner, F. C., Robin, C. and Alblas, J. (2019). A human hematopoietic niche model supporting hematopoietic stem and progenitor cells in vitro. *Adv. Healthc. Mater.* **8**, 1-14. doi:10.1002/adhm.201801444

Buenrostro, J. D., Corces, M. R., Lareau, C. A., Wu, B., Schep, A. N., Aryee, M. J., Majeti, R., Chang, H. Y. and Greenleaf, W. J. (2018). Integrated single-cell analysis maps the continuous regulatory landscape of human hematopoietic differentiation. *Cell.* **173**, 1535-1548.e16. doi:10.1016/j.cell.2018.03.074

Calvi, L. M., Spencer, J. A., Yeh, S.-C. A., Turcotte, R., Kokkaliaris, K. D., Panero, R., Ramos, A., Guo, G., Seyedhassantehrani, N., Esipova, T. V. et al. (2003). Osteoblastic cells regulate the haematopoietic stem cell niche. *Nature* **425**, 841-846. doi:10.1038/nature02041.1

Chang, J. T., Palanivel, V. R., Kinjyo, I., Schambach, F., Intlekofer, A. M., Banerjee, A., Longworth, S. A., Vinup, K. E., Mrass, P., Oliaro, J. et al. (2007). Asymmetric T lymphocyte division in the initiation of adaptive immune responses. *Science* **315**, 1687-1691. doi:10.1126/science.1139393

Christodoulou, C., Spencer, J. A., Yeh, S.-C. A., Turcotte, R., Kokkaliaris, K. D., Panero, R., Ramos, A., Guo, G., Seyedhassantehrani, N., Esipova, T. V. et al. (2020). Live-animal imaging of native haematopoietic stem and progenitor cells. *Nature* **578**, 278-283. doi:10.1038/s41586-020-1971-z

Cicalese, A., Bonizzi, G., Pasi, C. E., Faretta, M., Ronzoni, S., Giulini, B., Brisken, C., Minucci, S., Di Fiore, P. P. and Pelicci, P. G. (2009). The tumor suppressor p53 regulates polarity of self-renewing divisions in mammary stem cells. *Cell* **138**, 1083-1095. doi:10.1016/j.cell.2009.06.048

Colmone, A., Amorim, M., Pontier, A. L., Wang, S., Jablonski, E. and Sipkins, D. A. (2008). Leukemic cells create bone marrow niches that disrupt the behavior of normal hematopoietic progenitor cells. *Science* **322**, 1861-1866. doi:10.1126/science.1164390

Daley, W. P. and Yamada, K. M. (2013). ECM-modulated cellular dynamics as a driving force for tissue morphogenesis. *Curr. Opin Genet. Dev.* **23**, 408-414. doi:10.1016/j.gde.2013.05.005

De La Roche, M., Asano, Y. and Griffiths, G. M. (2016). Origins of the cytolytic synapse. *Nat. Rev. Immunol.* **16**, 421-432. doi:10.1038/nri.2016.54

Douanne, T. and Griffiths, G. M. (2021). Cytoskeletal control of the secretory immune synapse. *Curr. Opin. Cell Biol.* **71**, 87-94. doi:10.1016/j.ceb.2021.02.008

Florian, M. C., Klose, M., Sacma, M., Jablanovic, J., Knudson, L., Nattamai, K. J., Marka, G., Vollmer, A., Soller, K., Sakk, V. et al. (2018). Aging alters the epigenetic asymmetry of HSC division. *PLoS Biol.* **16**, e2003389. doi:10.1371/journal.pbio.2003389

Fonseca, A.-V., Freund, D., Bornhäuser, M. and Corbeil, D. (2010). Polarization and migration of hematopoietic stem and progenitor cells rely on the RhoA/ROCK I pathway and an active reorganization of the microtubule network. *J. Biol. Chem.* **285**, 31661-31671. doi:10.1074/jbc.M110.145037

Glait-Santar, C., Desmond, R., Feng, X., Bat, T., Chen, J., Heuston, E., Mizukawa, B., Mulloy, J. C., Bodine, D. M., Larochelle, A. et al. (2015). Functional niche competition between normal hematopoietic stem and progenitor cells and myeloid leukemia cells. *Stem Cells* **33**, 3635-3642. doi:10.1002/stem.2208

Glaser, D. E., Curtis, M. B., Sariano, P. A., Rollins, Z. A., Shergill, B. S., Anand, A., Deely, A. M., Shirure, V. S., Anderson, L., Lowen, J. M. et al. (2022). Organ-on-a-chip model of vascularized human bone marrow niches. *Biomaterials* **280**, 121245. doi:10.1016/j.biomaterials.2021.121245

Görgens, A., Ludwig, A.-K., Möllmann, M., Krawczyk, A., Dürig, J., Hanenberg, H., Horn, P. and Giebel, B. (2014). Multipotent hematopoietic progenitors divide asymmetrically to create progenitors of the lymphomyeloid and erythromyeloid lineages. *Stem Cell Rep.* **3**, 1058-1072. doi:10.1016/j.stemcr.2014.09.016

Ito, K., Turcotte, R., Cui, J., Zimmerman, S. E., Pinho, S., Mizoguchi, T., Arai, F., Runnels, J. M., Alt, C., Teruya-Feldstein, J. et al. (2016). Self-renewal of a

purified Tie2+ hematopoietic stem cell population relies on mitochondrial clearance. *Science* **354**, 1156-1160. doi:10.1126/science.aaf5530

Kahn, J., Byk, T., Jansson-Sjostrand, L., Petit, I., Shivtiel, S., Nagler, A., Hardan, I., Deutsch, V., Gazit, Z., Gazit, D. et al. (2004). Overexpression of CXCR4 on human CD34+ progenitors increases their proliferation, migration, and NOD/SCID repopulation. *Blood* **103**, 2942-2949. doi:10.1182/blood-2003-07-2607

Kiger, A. A., Jones, D. L., Schulz, C., Rogers, M. B. and Fuller, M. T. (2001). Stem cell self-renewal specified by JAK-STAT activation in response to a support cell cue. *Science* **294**, 2542-2545. doi:10.1126/science.1066707

Kräter, M., Jacobi, A., Otto, O., Tietze, S., Müller, K., Poitz, D. M., Palm, S., Zinna, V. M., Biehain, U., Wobus, M. et al. (2017). Bone marrow niche-mimetics modulate HSPC function via integrin signaling. *Sci. Rep.* **7**, 2549. doi:10.1038/s41598-017-02352-5

Kuang, S., Kuroda, K., Le Grand, F. and Rudnicki, M. A. (2007). Asymmetric self-renewal and commitment of satellite stem cells in muscle. *Cell* **129**, 999-1010. doi:10.1016/j.cell.2007.03.044

Lapidot, T., Dar, A. and Kollet, O. (2005). How do stem cells find their way home? *Blood* **106**, 1901-1910. doi:10.1182/blood-2005-04-1417

Liang, R., Arif, T., Kalmykova, S., Kasianov, A., Lin, M., Menon, V., Qiu, J., Bernitz, J. M., Moore, K., Lin, F. et al. (2020). Restraining lysosomal activity preserves hematopoietic stem cell quiescence and potency. *Cell Stem Cell* **26**, 359-376.e7. doi:10.1016/j.stem.2020.01.013

Lo Celso, C., Fleming, H. E., Wu, J. W., Zhao, C. X., Miake-Lye, S., Fujisaki, J., Côté, D., Rowe, D. W., Lin, C. P. and Scadden, D. T. (2009). Live-animal tracking of individual haematopoietic stem/progenitor cells in their niche. *Nature* **457**, 92-96. doi:10.1038/nature07434

Loeffler, D., Wehling, A., Schneiter, F., Zhang, Y., Müller-Bötticher, N., Hoppe, P. S., Hilsenbeck, O., Kokkaliaris, K. D., Endele, M. and Schroeder, T. (2019). Asymmetric lysosome inheritance predicts activation of haematopoietic stem cells. *Nature* **573**, 426-429. doi:10.1038/s41586-019-1531-6

Loeffler, D., Schneiter, F., Wang, W., Wehling, A., Kull, T., Lengerke, C., Manz, M. G. and Schroeder, T. (2022). Asymmetric organelle inheritance predicts human blood stem cell fate. *Blood* **139**, 2011-2023. doi:10.1182/blood.2020009778

Lord, S. J., Velle, K. B., Mullins, R. D. and Fritz-Laylin, L. K. (2020). SuperPlots: communicating reproducibility and variability in cell biology. *J. Cell Biol.* **219**, e202001064. doi:10.1083/JCB.202001064

Mesa, K. R., Kawaguchi, K., Cockburn, K., Gonzalez, D., Boucher, J., Xin, T., Klein, A. M. and Greco, V. (2018). Homeostatic epidermal stem cell self-renewal is driven by local differentiation. *Cell Stem Cell* **23**, 677-686.e4. doi:10.1016/j.stem.2018.09.005

Miao, R., Chun, H., Feng, X., Gomes, A. C., Choi, J. and Pereira, J. P. (2022). Competition between hematopoietic stem and progenitor cells controls hematopoietic stem cell compartment size. *Nat. Commun.* **13**, 4611. doi:10.1038/s41467-022-32228-w

Nakahara, F., Borger, D. K., Wei, Q., Pinho, S., Maryanovich, M., Zahalka, A. H., Suzuki, M., Cruz, C. D., Wang, Z., Xu, C. et al. (2019). Engineering a haematopoietic stem cell niche by revitalizing mesenchymal stromal cells. *Nat. Cell Biol.* **21**, 560-567. doi:10.1038/s41556-019-0308-3

Nervi, B., Ramirez, P., Rettig, M. P., Uy, G. L., Holt, M. S., Ritchey, J. K., Prior, J. L., Piwnica-Worms, D., Bridger, G., Ley, T. J. et al. (2009). Chemosensitization of acute myeloid leukemia (AML) following mobilization by the CXCR4 antagonist AMD3100. *Blood* **113**, 6206-6214. doi:10.1182/blood-2008-06-162123

Notta, F., Doulatov, S., Laurenti, E., Poeppl, A., Jurisica, I. and Dick, J. E. (2011). Isolation of single human hematopoietic stem cells capable of long-term multilineage engraftment. *Science* **333**, 218-221. doi:10.1126/science.1201219

Orkin, S. H. and Zon, L. I. (2008). Hematopoiesis: an evolving paradigm for stem cell biology. *Cell* **132**, 631-644. doi:10.1016/j.cell.2008.01.025

Pham, K., Shimoni, R., Charnley, M., Ludford-Menting, M. J., Hawkins, E. D., Ramsbottom, K., Oliaro, J., Izon, D., Ting, S. B., Reynolds, J. et al. (2015). Asymmetric cell division during T cell development controls downstream fate. *J. Cell Biol.* **210**, 933-950. doi:10.1083/jcb.201502053

Pinho, S. and Frenette, P. S. (2019). Haematopoietic stem cell activity and interactions with the niche. *Nat. Rev. Mol. Cell Biol.* **20**, 303-320. doi:10.1038/s41580-019-0103-9

Schofield, R. (1978). The relationship between the spleen colony-forming cell and the haemopoietic stem cell. *Blood Cells* **4**, 7-25.

Song, X., Zhu, C.-H., Doan, C. and Xie, T. (2002). Germline stem cells anchored by adherens junctions in the Drosophila ovary niches. *Science* **296**, 1855-1857. doi:10.1126/science.1069871

Souquet, B., Opitz, M., Vianay, B., Brunet, S. and Théry, M. (2021). Manufacturing a bone marrow-on-a-chip using maskless photolithography. *Methods Mol. Biol.* **2308**, 263-278. doi:10.1007/978-1-0716-1425-9_20

Spoo, A. C., Luübbert, M., Wierda, W. G. and Burger, J. A. (2007). CXCR4 is a prognostic marker in acute myelogenous leukemia. *Blood* **109**, 786-791. doi:10.1182/blood-2006-05-024844

Tajbakhsh, S., Rocheteau, P. and Le Roux, I. (2009). Asymmetric cell divisions and asymmetric cell fates. *Ann. Rev. Cell Dev. Biol.* **25**, 671-699. doi:10.1146/annurev.cellbio.24.110707.175415

Tak, T., Prevedello, G., Simon, G., Paillon, N., Benlabiod, C., Marty, C., Plo, I., Duffy, K. R. and Perié, L. (2021). Hspcs display within-family homogeneity in differentiation and proliferation despite population heterogeneity. *eLife* **10**, e60624. doi:10.7554/eLife.60624

Ting, S. B., Deneault, E., Hope, K., Cellot, S., Chagraoui, J., Mayotte, N., Dorn, J. F., Laverdure, J.-P., Harvey, M., Hawkins, E. D. et al. (2012). Asymmetric segregation and self-renewal of hematopoietic stem and progenitor cells with endocytic Ap2a2. *Blood* **119**, 2510-2522. doi:10.1182/blood-2011-11-393272

Van Der Velde-Zimmermann, D., Verdaasdonk, M. A. M., Rademakers, L. H. P. M., De Weger, R. A., Van den Tweel, J. G. and Joling, P. (1997). Fibronectin distribution in human bone marrow stroma: matrix assembly and tumor cell adhesion via $\alpha 5\beta 1$ integrin. *Exp. Cell Res.* **230**, 111-120. doi:10.1006/excr.1996.3405

Vannini, N., Campos, V., Girotra, M., Trachsel, V., Rojas-Sutterlin, S., Tratwal, J., Ragusa, S., Stefanidis, E., Ryu, D., Rainer, P. Y. et al. (2019). The NAD-Booster Nicotinamide Riboside Potently Stimulates Hematopoiesis through Increased Mitochondrial Clearance. *Cell Stem Cell* **24**, 405-418.e7. doi:10.1016/j.stem.2019.02.012

Venkei, Z. G. and Yamashita, Y. M. (2018). Emerging mechanisms of asymmetric stem cell division. *J. Cell Biol.* **217**, 3785-3795. doi:10.1083/jcb.201807037

Wagner, W., Wein, F., Roderburg, C., Saffrich, R., Faber, A., Krause, U., Schubert, M., Benes, V., Eckstein, V., Maul, H. et al. (2007). Adhesion of hematopoietic progenitor cells to human mesenchymal stem cells as a model for cell-cell interaction. *Exp. Hematol.* **35**, 314-325. doi:10.1016/j.exphem.2006.10.003

Wilson, A. and Trumpp, A. (2006). Bone-marrow haematopoietic-stem-cell niches. *Nat. Rev. Immunol.* **6**, 93-106. doi:10.1038/nri1779

Wu, M., Kwon, H. Y., Rattis, F., Blum, J., Zhao, C., Ashkenazi, R., Jackson, T., Gaiano, N., Oliver, T. and Reya, T. (2007). Imaging hematopoietic precursor division in real time. *Cell Stem Cell* **1**, 541-554. doi:10.1016/j.stem.2007.08.009

Wu, Q., Zhang, J., Kumar, S., Shen, S., Kincaid, M., Johnson, C. B., Zhang, Y. S., Turcotte, R., Alt, C., Ito, K. et al. (2024). Resilient anatomy and local plasticity of naive and stress haematopoiesis. *Nature* **627**, 839-846. doi:10.1038/s41586-024-07186-6

Xiao, M., Inal, C. E., Parekh, V. I., Li, X. H. and Whitnall, M. H. (2009). Role of NF-κB in hematopoietic niche function of osteoblasts after radiation injury. *Exp. Hematol.* **37**, 52-64. doi:10.1016/j.exphem.2008.09.001

Yu, J., Choi, S., Kim, H., Lee, N., Yun, H., Kim, S., Jeong, S.-T. and Rho, J. (2017). Generation of an osteoblast-based artificial niche that supports in vitro B lymphopoiesis. *Exp. Mol. Med.* **49**, e400-e412. doi:10.1038/emm.2017.189

Zanetti, C. and Krause, D. S. (2020). 'Caught in the net': the extracellular matrix of the bone marrow in normal hematopoiesis and leukemia. *Exp. Hematol.* **89**, 13-25. doi:10.1016/j.exphem.2020.07.010

Zhang, J., Wu, Q., Johnson, C. B., Pham, G., Kinder, J. M., Olsson, A., Slaughter, A., May, M., Weinhaus, B., D'Alessandro, A. et al. (2021). In situ mapping identifies distinct vascular niches for myelopoiesis. *Nature* **590**, 457-462. doi:10.1038/s41586-021-03201-2

Zimdahl, B., Ito, T., Blevins, A., Bajaj, J., Konuma, T., Weeks, J., Koechlein, C. S., Kwon, H. Y., Arami, O., Rizzieri, D. et al. (2014). Lis1 regulates asymmetric division in hematopoietic stem cells and in leukemia. *Nat. Genet.* **46**, 245-252. doi:10.1038/ng.2889